CHAPTER 16

ARM Solar and Infrared Broadband and Filter Radiometry

JOSEPH J. MICHALSKY

NOAA Earth System Research Laboratory, Boulder, Colorado

CHARLES N. LONG

Pacific Northwest National Laboratory, Richland, Washington

1. Introduction

Two papers published in the early 1990s comparing radiation transfer codes for the infrared (Ellingson et al. 1991) and for the solar (Fouquart et al. 1991) irradiance concluded that many of the radiation transfer codes (parameterized to reduce run time) used in climate models did not agree with state-of-the-art line-by-line radiative transfer codes; for the most part line-by-line codes agreed with one another. However, the measurements to confirm that the radiative fluxes produced by these line-by-line codes represented truth were unavailable. The Spectral Radiation Experiment (SPECTRE), a 25-day experiment in the fall of 1991, (Ellingson and Wiscombe 1996) was conducted near Coffeyville, Kansas, to simultaneously obtain surface radiation measurements and the most important of the inputs needed for these radiative transfer models, including temperature, humidity, aerosol, and cloud profiles. The ARM Program greatly expanded this initial effort to include a range of climates and to acquire at least 10 years of measurements with a focus on improving the number and the quality of the measured inputs needed for the models and improving the quality of the radiation measurements and the radiative transfer models.

The ARM Program and Baseline Surface Radiation Network (BSRN; Ohmura et al. 1998) matured together. Ellsworth Dutton, who played a significant role in the ARM Program, also served as the BSRN project manager for BSRN's first 20 years. ARM was focused on all aspects of trying to close the problem between radiative transfer models and radiation measurements using measured model inputs. BSRN was focused primarily on providing state-of-the-art broadband solar and infrared measurements at sites throughout the world that represented every type of climate. The BSRN data were intended for satellite and climate model validation and for the detection of long-term trends. Consequently, both programs benefited from each other's research efforts to improve solar and infrared radiometry. In 1990, estimates of the standard uncertainty for global horizontal, direct normal, diffuse horizontal solar irradiance, and downwelling global infrared irradiance were 15, 3, 10, and 30 $W\,m^{-2}$, respectively. The goal of BSRN was to reduce these broadband measurement uncertainties to 5, 2, 5, and 20 $W\,m^{-2}$ (Ohmura et al. 1998). Most of these goals have been met, and in some cases exceeded, through efforts in both ARM and BSRN. The radiation measurements of ARM adhere to the strict specifications of the BSRN, and five ARM sites report their data to the BSRN archive making up 10% of the total number of BSRN sites.

This chapter describes the history of ARM's ground-based measurements of broadband solar and broadband infrared radiation first, followed by a description of ARM's spectral solar measurements that are made with interference filter radiometers. Spectral measurements made using spectrometers are discussed in Mlawer and Turner (2016, chapter 14).

Measurements of the broadband (i.e., the spectrally integrated solar spectrum or shortwave; 280–4000 nm) that come directly from the sun without being absorbed or scattered are measurements of direct normal irradiance

Corresponding author address: Joseph J. Michalsky, NOAA/University of Colorado Cooperative Institute for Research in Environmental Sciences, 325 Broadway, Boulder, CO 80305.
E-mail: joseph.michalsky@noaa.gov

DOI: 10.1175/AMSMONOGRAPHS-D-15-0031.1

(DNI) and are made with a pyrheliometer mounted on a solar tracker to follow the sun. Measurements of skylight [diffuse horizontal irradiance (DHI)] arising from sunlight scattered by molecules, aerosols, and clouds are made with a pyranometer that has the DNI blocked by a shadow ball or disk mounted on a solar tracker. Unshaded pyranometers are mounted on a separate stand to measure all downwelling [global horizontal irradiance (GHI)] or all upwelling (reflected) solar radiation.

Broadband infrared (spectrally integrated from about 4000 to 50000 nm, or longwave) radiation from the sky is measured with a pyrgeometer that has a hemispheric field of view and an (approximate) cosine response. Broadband infrared emitted by the surface is measured with a horizontally mounted down-facing pyrgeometer. Only broadband infrared measurements are covered in this chapter; high-resolution spectral infrared measurements are discussed in Mlawer and Turner (2016, chapter 14).

Shortwave spectral measurements are made with interference-filter radiometers that cover selected portions of the solar spectrum where silicon-based detectors are responsive (300–1100 nm). One exception to this is the ARM Aeronet Robotic Network (AERONET) Cimel sunphotometers that have one channel at 1640 nm that uses an indium gallium arsenide (InGaAs) detector. The ARM Program primarily uses these narrowband spectral measurements to determine the spectral dependence of aerosol optical depth, cloud optical depth, and surface spectral albedo.

These broadband solar and infrared upwelling and downwelling irradiance measurements are made at the ARM's central facilities and at extended sites. Downwelling narrowband spectral measurements are made at all of the central and extended facilities. At the Southern Great Plains (SGP) central facility only, upwelling measurements are made with multifilter rotating shadowband radiometer (MFRSR) heads, referred to as the multifilter radiometer (MFR), in order to measure spectral albedo. At the SGP there were 23 extended facilities covering 142 000 km^2 until 2009 when the areal coverage shrank to 22 500 km^2 and 16 sites. At the North Slope of Alaska (NSA) site, there was the central facility near Barrow and one extended facility near Atqasuk. The Tropical Western Pacific (TWP) site had only central facilities on Nauru Island; in Manus, Papua New Guinea; and in Darwin, Australia. The ARM Mobile Facilities (AMFs) spend months to a year at selected sites. AMFs have the same radiation measurement suite as found at the central facilities of the fixed ARM sites.

NSA and AMF deployments in cold regions present special problems for radiometry. Ice buildup on instruments is the primary issue. A 2-yr intensive operational period (IOP), led by Scott Richardson, was conducted beginning in 2007 and ending in 2009 to study different techniques to heat and ventilate radiometers to keep the ice from forming yet minimizing the effects on the integrity of the measurements. Although improvements have been made, Arctic radiometry continues to be a challenge.

This chapter includes a discussion of specific broadband instruments used for measurements, their calibrations, and changes to the instrumentation including the data logging. Uncertainties in the field measurements are covered. A few of the major results using these measurements will be highlighted. Spectral measurements are discussed following the broadband sections including the instruments used, uncertainties, and a few significant results based on these measurements. Albedo measurements are covered only briefly since these calculated quantities are only recently beginning to be used. Note, some of the topics discussed in this chapter are also covered, in more detail or with a different emphasis, by Mlawer and Turner (2016, chapter 14), McFarlane et al. (2016, chapter 20), and McComiskey and Ferrare (2016, chapter 21).

2. Broadband solar measurements

Up-looking pyranometers are mounted about 2 m above the surface and their domes are ventilated with ambient air to reduce dust and dew buildup. The broadband solar that is reflected by the surface is measured with a down-facing, horizontally mounted pyranometer that is not ventilated, and albedo is determined by taking the ratio of this measurement to the downwelling GHI. The most accurate GHI is obtained, not from the unshaded pyranometer, but from summing DNI and DHI components:

$$\mathrm{GHI} = \mathrm{DNI} \times \cos(\mathrm{SZA}) + \mathrm{DHI}, \qquad (16\text{-}1)$$

where solar zenith angle (SZA) is the angle between the zenith and the sun's direction. The unshaded pyranometer measures global irradiance; however, this measurement is less accurate and used mainly to compare to the component sum in Eq. (16-1) for the purpose of detecting tracker failure or sensor blockage. The down-facing pyranometer is mounted near the top of a 10-m tower. The surface under the tower is chosen to be uniform in the near vicinity (out to about 4 times the height of the sensor). The solar spectrum includes all radiation between 280 and 4000 nm. Pyrheliometers use a glass window that includes this range, but pyranometer measurements often respond over a somewhat smaller range (typically, 300–3000 nm). There are small solar contributions from wavelengths that are shorter than 300 nm and longer than 3000 nm. However, since pyranometers are calibrated by comparing to a full-spectrum instrument, their response is very nearly proportional to the full solar spectrum. Pyranometers measure

hemispheric radiation with a sensor that has an (approximate) cosine response, and pyrheliometers in ARM measure direct beam radiation with a field of view of 5.7° that necessarily includes some diffuse radiation in the sun's aureole.

Measurements of global (i.e., total) horizontal solar radiation are made with the Eppley model precision spectral pyranometer (PSP). PSPs are designated first-class instruments according to World Meteorological Organization (WMO) specifications (Coulson and Howell 1980). ARM measurements of diffuse radiation used Eppley PSPs until it was (re)discovered (Gulbrandsen 1978) that there is a significant offset with this instrument (Bush et al. 2000; Dutton et al. 2001). In 2001 all of the Eppley model PSPs were replaced with the Eppley model 8–48s for DHI measurements at all ARM sites worldwide. The 8–48 (i.e., black and white) pyranometer has the desirable property that its offset is nearly zero (Michalsky et al. 2003). The Eppley PSP is now only used for the GHI backup measurement to the BSRN-preferred component summation. The preference for summation of observations from two radiometers [Eq. (16-1)] versus a single pyranometer measurement is explained in chapters 5 and 6 of Vignola et al. (2012). In essence, the uncertainties are reduced by at least a factor of 50% when using the component sum for global irradiance even compared to GHI measurements obtained with top-of-the-line pyranometers [see chapter 6 in Vignola et al. (2012)]. The current estimates of 95% uncertainties of GHI are about ±3% under very good conditions; therefore, a reasonable estimate of uncertainty for routine field operations is higher at ±4%. The DHI is measured with a current 95% uncertainty of about ±2% for very good conditions and ±3% under field conditions.

The Eppley model normal incidence pyrheliometer (NIP) is used to measure broadband direct normal solar irradiance in ARM. This instrument also received a first-class designation from the WMO (Coulson and Howell 1980). This instrument is mounted on a solar tracker (Kipp and Zonen 2AP; http://www.kippzonen.com/?product/2141/2AP.aspx) to follow the sun to better than 1°. This same tracker is used to shade the pyranometer used for DHI. In a recent paper Michalsky et al. (2011) quantified the uncertainty of measurements made with several pyrheliometers including the Eppley NIP used in the ARM Program. The comparison was noteworthy in that the measurements were made in typical midlatitude field conditions in all seasons. The results indicated that the Eppley NIP has a 95% uncertainty of ±1.3%, which is actually better than the 2% uncertainty suggested by the manufacturer. However, three commercial pyrheliometers in this study had 95% uncertainties of around 0.7%.

The ARM Data Archive (www.archive.arm.gov) contains broadband solar radiation data that were taken using a datalogger that sampled once every 20 s at the SGP sites until 1997. New Campbell loggers were exchanged for these early ones to allow 2-s sampling with 60-s averaging beginning in 1997. In 2012 a newer version of the loggers permitted a step up to 1-s sampling with 60-s averaging at the SGP sites. All TWP, NSA, and ARM Mobile Facility sites used loggers with 1-s sampling and 60-s averaging from the outset since they sampled fewer signals than the radiation facilities at the SGP. As stated above, the diffuse measurements were made using the Eppley 8–48 after 2001; the PSP measurements of diffuse and global irradiance that appear in the archive have been offset corrected to the beginning of the datasets. For the best set of measurements with all corrections implemented, the archive data streams that include "qcrad" in the data stream title should be retrieved; the title "sgpqcradbrs1longC1.s1," for example, contains the last few years of quality-controlled data up to the current measurements.

3. Broadband solar calibrations

All solar measurements in ARM are ultimately tied to the World Radiometric Reference (WRR) that is maintained at the Physikalisch-Meteorologisches Observatorium Davos and World Radiation Center (http://www.pmodwrc.ch). The WRR for DNI consists of several absolute cavity radiometers that have been carefully characterized (Fröhlich et al. 1995); currently, it includes six radiometers from five different manufacturers. Operationally, an absorbing cavity within the radiometer is heated when the sun impinges on the cavity through an aperture with a precisely defined area. A shutter is closed and then the cavity is heated by an electrical current to the same temperature it had with the sun shining into the cavity. The solar irradiance is then calculated as the electrical power to heat the cavity in watts divided by the area of the aperture with small corrections applied, based on the characterization of the cavity radiometer.

Every five years ARM cavity radiometers, which serve as secondary standards for ARM shortwave measurements, travel to Davos, Switzerland, and are calibrated against the WRR at the International Pyrheliometer Comparison (IPC). On the off years, the National Renewable Energy Laboratory (NREL) in Golden, Colorado, hosts a comparison [NREL Pyrheliometer Comparison (NPC)] using several cavity radiometers that are calibrated at the quinquennial IPCs in Davos. Cavity radiometers are not used in ARM because they are more than 10 times the cost of thermopile pyrheliometers and

FIG. 16-1. The Radiometric Calibration Facility at the ARM Southern Great Plains site near Billings, Oklahoma; close-up of pyranometers being calibrated at the facility.

operate with an open cavity, which makes it impractical to use for continuous unattended measurements because dust and other debris may get into the cavity and contaminate the measurements.

The diffuse reference consists of three Eppley model 8–48 pyranometers that are calibrated against the WRR-traceable cavity radiometers using a procedure known as the shade/unshade technique. In this method, a horizontally mounted pyranometer under clear and stable irradiance conditions is shaded and then unshaded from the direct sun using a blocker of the same angular diameter as the angular diameter of a cavity radiometer (5°). The difference in voltages from the pyranometer for the two configurations is equated to the cavity-measured direct irradiance after multiplication by the cosine (SZA). These measurements are repeated at several SZAs, but the average value near the SZA of 45° is typically used for the single-number calibration factor for the pyranometer. The average of three 8–48s is used for the diffuse horizontal standard irradiance.

The ARM Radiometric Calibration Facility (RCF; see Fig. 16-1) was constructed to calibrate the many pyranometers and pyrheliometers used at the permanent and mobile ARM facilities. These radiometers are calibrated en masse in Broadband Outdoor Radiation Calibrations (BORCALs; Myers et al. 2002) performed at the ARM SGP site by comparing pyrheliometer voltage outputs with the ARM cavity radiometer irradiances and by comparing pyranometer voltage outputs with the component sum irradiance, that is,

$$\text{global irradiance reference} = \text{cavity} \times \cos(\text{SZA}) + \text{reference diffuse}. \quad (16\text{-}2)$$

Measurements are made under clear, stable conditions with the DNI over 700 W m^{-2}, but the single calibration factor is based on measurements near 45°SZA. All broadband calibrations for ARM are performed at the SGP RCF and instruments are shipped to the other ARM sites for deployment. In fact, the RCF is a true user facility serving as the site for the first International Pyrgeometer and Absolute Sky-scanning Radiometer Comparison (Philipona et al. 2001) and the site of three diffuse irradiance IOPs (Michalsky et al. 2003, 2005, 2007).

4. Broadband infrared measurements

Downwelling infrared radiation from the sky and upwelling infrared from the surface is measured using Eppley model precision infrared radiometer (PIR) pyrgeometers oriented horizontally. The down-looking pyrgeometer is mounted at about the 10-m level. Up-looking pyrgeometers are mounted on solar trackers at 2 m above the ground and are shaded from direct solar radiation to minimize solar contributions to the signals that may arise from pinholes in the silicon dome covering these instruments or from shortwave leakage of the interference filter covering the PIR dome. The dome of the up-looking PIR is ventilated with ambient air.

5. Broadband infrared calibrations

The current calibrations used in ARM for the pyrgeometers are those provided by the manufacturer Eppley Laboratory, Inc. A pyrgeometer produces three electrical signals: a thermopile signal, a dome temperature signal, and a case temperature signal. The data are converted to infrared irradiance I_{ir} using

$$I_{\text{ir}} = V_{\text{thermo}}/C + \sigma T_B^4 - k\sigma(T_D^4 - T_B^4), \quad (16\text{-}3)$$

where σ is the Stefan–Boltzmann constant, V_{thermo} is the thermopile voltage, T_B and T_D are temperatures (K) of the case (or body) and dome, respectively, and C and k are calibration constants. Eppley's calibration procedure

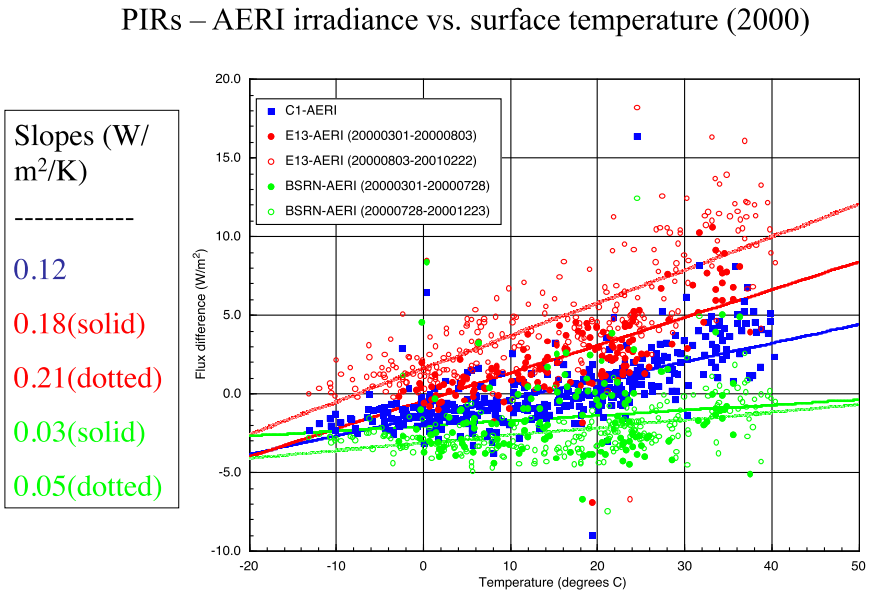

FIG. 16-2. Collocated AERI-based estimated LW irradiance subtracted from PIR-based measured irradiances for three PIRs designated C1, E13 (two time periods), and BSRN (two time periods) as a function of ambient temperature. Slopes are to the bottom left of the figure.

is outlined in chapter 10 of Vignola et al. (2012). The pyrgeometer peers into a blackbody whose temperature is controlled by a circulating water bath first at 5°C and then at 15°C. In about five minutes after being positioned to look into the blackbody, the instrument and blackbody come to equilibrium and T_B and T_D are at the same temperature. Therefore,

$$C = \frac{V_{\text{thermo}}}{\sigma(T_{\text{BB}}^4 - T_B^4)}, \tag{16-4}$$

where T_{BB} is the blackbody temperature at 5°C and subsequently 15°C. The calibration constant is based on the average of its value at the two temperature settings of the blackbody. The constant k in Eq. (16-2) is assigned a value of 4 by Eppley.

Using a constant value of 4 for k may not be appropriate since that value was assigned for KRS-5 domes that are no longer used for the Eppley PIR; all PIR domes in ARM are silicon, and the manufacturer (via private communication) now suggests that 3.5 may be a more appropriate constant for k. Other blackbody calibration methods solve for the value of k [e.g., see chapter 10 of Vignola et al. (2012)]. In one study, for example, Philipona et al. (2001) found a range for k of 2.75 to 3.64 for a set of six PIRs that were calibrated at the World Radiation Center in Davos, Switzerland (www.pmodwrc.ch).

Figure 16-2 above is a plot of an Atmospheric Emitted Radiance Interferometer (AERI)-based broadband irradiance estimate subtracted from PIR measurements of downwelling irradiance. The AERI (Knuteson et al. 2004; Turner et al. 2016, chapter 13) measures spectral radiance that is converted to infrared irradiances by filling in missing portions of the spectrum (minor corrections) and estimating the angular dependence of the radiance (Marty et al. 2003). While there are uncertainties in the AERI-based irradiance estimates, and this method cannot to be considered a standard, the fact that there are differences in slopes in Fig. 16-2 for the three independent PIR measurements collocated with the AERI points to an issue with pyrgeometer calibration since they are not producing the same irradiances on average. We suspect that the issue is the assignment of a fixed value for k in Eq. (16-3). This suspicion is based on our ability to reproduce the value of the other calibration constant c with great reliability, and based on our and others' experience that PIRs calibrated in other black bodies often have k values different from the fixed value of 4 used for the ARM PIRs, as indicated in the previous paragraph.

ARM's attempt to perform its own blackbody calibrations in early 2001 (Reda and Stoffel 2001), using a newly constructed blackbody calibrator, produced an unrealistically large offset that was traced to nonuniform temperatures in the new blackbody cavity (Stoffel et al. 2006). The ARM Radiation Focus Group decided to change to an outdoor calibration technique that compares to pyrgeometers that have been calibrated against the World Infrared Standard Group (WISG) in Davos, Switzerland. However, as of this writing the PIR

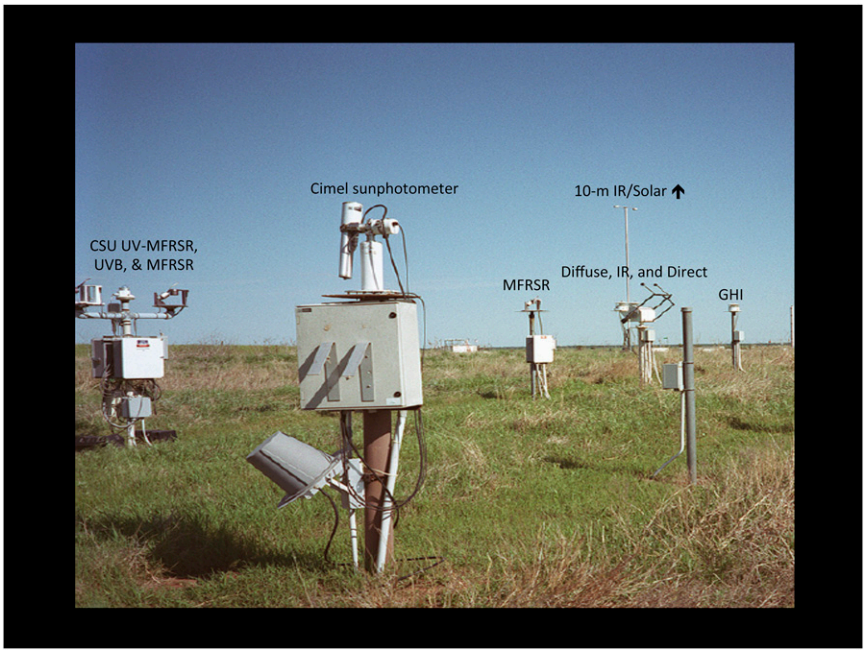

FIG. 16-3. The radiometer cluster at the ARM Southern Great Plains Central Facility.

measurements in the archive continue to be based on the original Eppley calibrations.

An interesting side note to the broadband infrared work is that the RCF at SGP was used in the First International Pyrgeometer and Absolute Sky-scanning Radiometer Comparison (IPASRC I; Philipona et al. 2001) and the ARM NSA site was used in IPASRC II (Marty et al. 2003) to establish the WISG that ARM will use for calibrations and that many radiation installations are already using for pyrgeometer calibrations.

6. Significant achievements in broadband radiometry

Figure 16-3, from the SGP site, shows most of the instruments that make the broadband and narrowband radiation measurements discussed in this chapter. The Cimel sunphotometer is shown in the foreground. A UV-MFRSR, a UVB broadband radiometer, and a visible MFRSR from Colorado State University are to the left. Diffuse and infrared downwelling measurements are made on the tracker identified by the two arms with black spheres at their ends (center right) that block the sun; this tracker also carries the solar direct normal instrument. To the right of the tracker is an unshaded pyranometer that makes the GHI measurement. The tower behind the tracker makes upwelling solar and infrared measured at 10 m. The archive of BSRN-quality radiation measurements beginning in 1993 at the SGP site and beginning in 1998 at the NSA and TWP sites is a significant achievement.

In the early years of the ARM Program, the Instantaneous Radiative Flux (IRF) working group was dedicated to improving measurements and radiative transfer models. Often this was done through quality measurement experiments where, for example, measured inputs to radiative transfer models were used to predict the measured irradiance. Finding explanations for any differences led to improved measured inputs, improved models, and improved radiation measurements. An example is provided in chapter 14 for spectral infrared radiance (Mlawer and Turner 2016, chapter 14; Turner et al. 2004), but comparisons of longwave and shortwave flux calculations with observations were also a prominent focus (e.g., Clough et al. 2000; Ricchiazzi et al. 1998; Michalsky et al. 2006). A few achievements are highlighted below.

a. Diffuse irradiance

Using data from the first ARM Enhanced Shortwave Experiment (ARESE), Kato et al. (1997) performed a careful study where they compared clear-sky radiation models with ARM measurements of direct normal and diffuse horizontal shortwave irradiances. Direct irradiances agreed well with the models with correct inputs of aerosol optical depth (AOD), water vapor column, and ozone column. Modeled diffuse irradiances using reasonable aerosol optical properties of absorption and scattering were consistently higher than DHI measurements by a significant margin. Halthore et al. (1998)

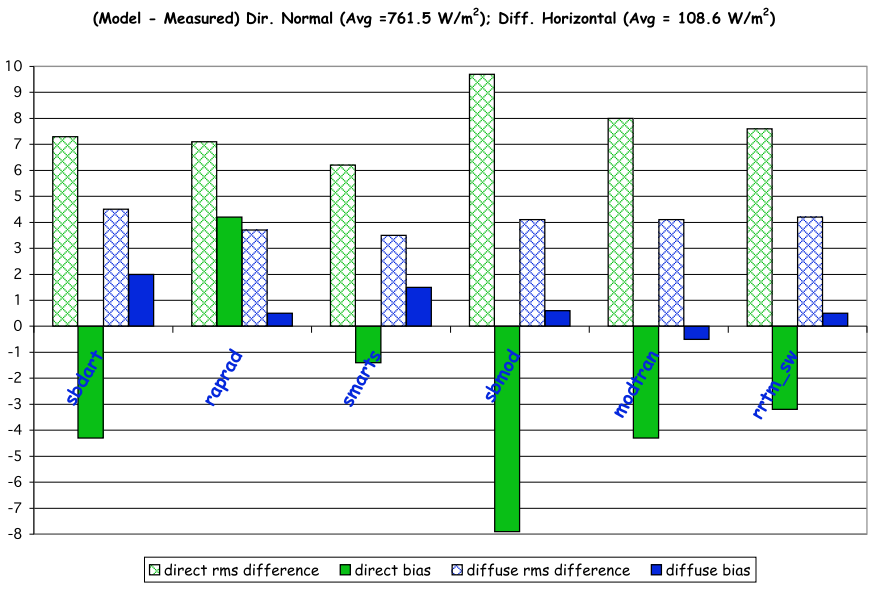

FIG. 16-4. Model minus measurement irradiance ($W\,m^{-2}$) for six models showing direct (green) and diffuse (blue) rms differences (hatched) and biases (solid). Note the mean direct and diffuse irradiances for the 30 cases are given in the figure title. From Michalsky et al. (2006).

reached a similar conclusion, finding consistently higher modeled diffuse irradiance than measured using sensible model inputs for the aerosol load and its optical properties. These results created a significant debate within the ARM (and larger) community: Was this bias between the observations and the model due to some missing absorption in the radiative transfer model or was this a problem with the radiation observations or the observations used to drive the radiative transfer model?

Papers by Bush et al. (2000) and Dutton et al. (2001) looked into offset problems with thermopile sensors and found that black disk detector pyranometers, such as the Eppley model PSP, had significant offsets. Dutton et al. (2001) found that these offsets were largest during the midafternoons of clear-sky days. In both Bush et al. (2000) and Dutton et al. (2001), a much earlier effort by Gulbrandsen (1978) was cited that clearly pointed to an early, but forgotten, recognition of this problem; this offset was largely ignored until measurements and models reached the level of accuracy occurring in the BSRN/ARM era. The Dutton et al. (2001) study led to the replacement of all Eppley model PSPs used for ARM DHI measurements with Eppley model 8–48s, which do not have significant offsets. PSPs were retained for the GHI backup measurements, and all measurements of GHI made with PSPs were corrected in the ARM archive. A detailed explanation of the correction used for the ARM PSPs is given in Younkin and Long (2004).

Halthore et al. (2004) followed these improvements to the diffuse measurements with a study that concluded that model and measurement agreement was much improved, but that there were differences at times that could only be explained by invoking highly absorbing but perhaps unrealistic aerosol absorption properties. In a comprehensive study, Michalsky et al. (2006) compared six shortwave radiation models with direct and diffuse measurements for 30 cases over a wide range of aerosol loads and SZAs during an aerosol intensive campaign at the SGP Central Facility. The 30-case average bias (model − measurement; see Fig. 16-4) for the direct normal ranged from a low of −1.0% to a high of +0.7% for an averaged DNI of $762\,W\,m^{-2}$. For the diffuse irradiance, the range was from −0.6% to +1.9% for an averaged DHI of $109\,W\,m^{-2}$. The improved agreement compared to Halthore et al. (2004) was attributed to having accurate AODs, reasonable single scattering albedos (SSA), and asymmetry parameters (AP) from in situ measurements, and good water vapor inputs for the model. However, the main cause of the good agreement in Michalsky et al. (2006) between the measurements and the model calculations was the change from using a broadband albedo, which was the same for all wavelengths, in the calculation to a six-band spectral albedo measurement with reasonable assumptions for the wavelength dependent interpolation and extrapolation; this change led to a 7% reduction of the diffuse irradiance in the model calculations.

A major improvement in radiation measurements was ARM's development of a standard procedure for calibrating the DHI; this standard did not exist prior to the

ARM Program. After three IOPs to find pyranometers with consistent behavior for diffuse measurements, Michalsky et al. (2007) proposed and demonstrated a procedure for developing a diffuse working standard that reduced the uncertainty of diffuse measurements. Those results apply to clear-sky measurements, which are arguably the most difficult diffuse measurements to make reliably. Clear skies with low aerosol burden have the lowest irradiance since aerosols increase the diffuse irradiance.

b. *Direct irradiance*

Under ideal circumstances, direct irradiance would be measured by windowless absolute cavity radiometers (Vignola et al. 2012). Since operating with an open cavity is not practical for long-term operations and cavity radiometers are expensive, pyrheliometers based on thermopile detectors are used for routine measurements. To determine the uncertainty of these instruments a comparison was conducted for nearly a year to compare pyrheliometers for all seasons under realistic field conditions. The results are reported in Michalsky et al. (2011). In general, DNIs are measured with better accuracy than is claimed by the manufacturer. The good news for ARM is that Eppley pyrheliometers that are used in ARM were found to have a 95% measurement uncertainty of ±1.3%, much better than the ±2.0% claimed by the manufacturer. However, three competitively priced pyrheliometer manufacturers had instruments with 95% uncertainties of about ±0.7%. This study, for the first time, provided a clear understanding of the uncertainty of this primary measurement made by ARM and the BSRN community as a whole.

c. *ARESE and ARESE II*

In 1995, three journal articles by Cess et al. (1995), Ramanathan et al. (1995), and Pilewskie and Valero (1995) appeared that suggested absorption in clouds was far greater than theoretical models predicted. Shortly after these publications, ARM mounted a campaign called the ARM Enhanced Shortwave Experiment (ARESE; Valero et al. 1997a) to measure radiation above and below clouds from aircraft flying in tandem and then to compare those measurements with radiation measurements when there were no clouds. The experiment, which was conducted in the fall of 1995, was marked by exceptionally clear weather; therefore, the analysis relied heavily on a single overcast day to estimate absorption in the clouds. Analyzing those data, Valero et al. (1997b) and Zender et al. (1997) found excess absorption consistent with the 1995 papers. Other experiments conducted elsewhere at about the same time by British researchers (Francis et al. 1997) and Japanese researchers (Asano et al. 2000) found that the measured absorption differed from theoretical calculations by less than 10% compared to the more than 50% deviation reported by Valero et al. (1997b) and Zender et al. (1997).

To resolve the issue, a second experiment called ARESE II (Valero et al. 2003), conducted in the winter of 2000, used three sets of radiometers on the aircraft that flew above the clouds of the ARM SGP central facility. Multiple sets of radiation measurements also were made at the surface of the central facility to calculate the net radiation at the surface that was compared with the net radiation measured at the aircraft. All ground and aircraft radiometers were calibrated to the same standard simultaneously (Michalsky et al. 2002) after the offset issues were found and dealt with by using zero offset radiometers or offset corrections. Ackerman et al. (2003), using two state-of-the-art radiative transfer models, analyzed the results on three cloudy days of ARESE II and found that measurements and models for the atmospheric absorption in the clouds agreed to within 10%, which was within the estimated model and measurement accuracy. Cloud absorption on the order of 50% more than model predictions was clearly not observed in this experiment. A good discussion of this appears in Kerr (2003) that emphasizes that both measurement and model improvement led to this result.

d. *Radiative flux analysis*

Long and Ackerman (2000) used ARM data to develop a technique to understand the effect of clouds on downwelling solar irradiance (GHI) at the surface. The technique uses the GHI and DHI time series to detect periods of clear (i.e., cloudless) skies. If a day's detected clear-sky period spans a sufficient range of SZA, the data are used to fit functions with the cosine of the SZA as the independent variable. The coefficients of the fit are then linearly interpolated between clear periods to produce continuous estimates of clear-sky GHI and DHI over that period. Since the predicted clear-sky irradiances are affected by whatever water vapor, aerosols, and other constituents are present, the irradiance differences (radiative effects) when clouds are present are only due to clouds; the assumption is that aerosol, water vapor, and the other constituents remain relatively constant over the day.

Figure 16-5 demonstrates the technique developed by Long and Ackerman (2000). The clear-sky global solar (GHI) model closely matches the measured global solar in the morning and the extrapolation assumes that a clear sky prevails the rest of the day. The deviations of the measured GHI from this model represent the clouds' effects on the radiation budget. The same argument holds for the diffuse solar (DHI) plotted in the blue colors.

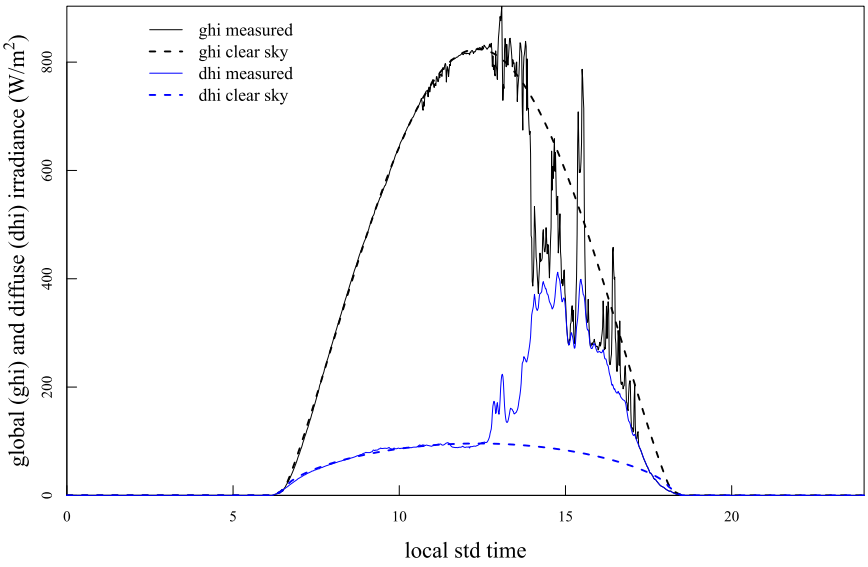

FIG. 16-5. Demonstration of radiative flux analysis where clear portion of morning is used to estimate what the rest of a clear-sky day's pattern in global and diffuse would be expected to follow if it remained clear. Deviations from the clear-sky global and diffuse are attributed to cloud radiative forcing.

Later, techniques were developed to produce continuous estimates of clear-sky downwelling infrared I_{ir} (Long and Turner 2008) irradiance, and upwelling solar and infrared (Long 2005) irradiance. These clear-sky estimates are used along with the corresponding measurements in various combinations to calculate the complete net radiative cloud forcing, and infer cloud macrophysical properties such as daylight fractional sky cover (Long et al. 2006), I_{ir} effective sky cover (Dürr and Philipona 2004), cloud optical depth (Barnard et al. 2008), cloud transmissivity, effective clear-sky emissivity, and sky brightness temperature.

Using the long-term surface radiation datasets available, several papers have used radiative flux analysis (RFA) estimates in model-measurement comparisons of surface radiation and cloud amounts. Wild et al. (2006) used RFA clear-sky results to test the general circulation models (GCMs) that participated in the atmospheric model intercomparison projects (AMIP I and AMIP II) and the model intercomparisons for the Fourth Assessment Report (AR4) of the Intergovernmental Panel on Climate Change (IPCC 2007), while Qian et al. (2012) tested the AR4 models' accuracy for cloud fraction and radiative effects. Zhang et al. (2010) show that the RFA-related suite of retrieved parameters allows for comparison of satellite and surface data sorted by when both are experiencing similar cloudiness, thus getting around many of the previous problems inherent in comparing values that represent differing spatial coverage, an age-old satellite–surface comparison issue.

The RFA data have been used in analyses of surface cloud effects and trends. Long et al. (2009) showed significant decadal brightening over the continental United States that is attributed to changes in cloudiness rather than changes in aerosol loading. For clear sky, the increase was manifested in the diffuse shortwave rather than the direct shortwave that would be expected for the documented decreased aerosol loading across the decade of the study. Mace et al. (2006) studied cloud radiative forcing at the ARM SGP site and comparisons to satellites, while Berg et al. (2011) studied surface radiative forcing specifically by single-layer shallow cumulous clouds at SGP. At the ARM NSA site Dong et al. (2010) studied the cloud radiative forcing climatology. In the ARM TWP sites Wang et al. (2011) used RFA cloud effects and sky-cover retrievals to show that the Madden–Julian oscillation is detected and quantified in the Manus, Papua New Guinea, site data; May et al. (2012) investigated the diurnal cycle of the Australian monsoon including cloudiness and radiative effects; and McFarlane et al. (2013) analyzed the climatology of surface cloud radiative effects, by cloud type, at all three TWP sites.

7. Spectral solar measurements for aerosol retrievals

a. Cimel sunphotometers

ARM solar spectral measurements have focused mainly on the retrievals of AOD and aerosol optical properties. In the late 1990s ARM became part of

AERONET (Holben et al. 1998) with the introduction of Cimel sunphotometers at the central facility sites in Oklahoma, Alaska, and on Nauru. The Cimel sunphotometers (see Fig. 16-3) are now at all ARM permanent central facilities and ARM mobile facilities; in addition, spares are kept for replacements. The spares are critical because it takes a month or more to calibrate the sunphotometers, which is done by sending the instrument to AERONET headquarters at the Goddard Space Flight Center in Greenbelt, Maryland. These spares fill significant gaps in the data stream that would otherwise be created. Calibration is via comparisons to other Cimel sunphotometers that have been calibrated at Mauna Loa Observatory in Hawaii using Langley plot analyses.

The wavelengths that are standard in all of the ARM Cimels are 340, 380, 440, 500, 675, 870, 940, 1020, and 1640 nm. All are used for AOD retrievals except the 940-nm channel, which is used to estimate the amount of water vapor in the column. Measurements to calculate AOD are made at every half air mass if the air mass is greater than 2, or every 15 min if the air mass is less than 2. The uncertainties for AOD are estimated at 0.01 to 0.02 (Gregory 2011). The four channels at 440, 675, 870, and 1020 nm are used to scan in the solar almucanter and in the solar-zenith plane measuring radiance at defined angles. These scans, occurring four times daily for each scan plane, are used, along with the direct spectral irradiance measurements, to retrieve AP (a measure of the forward versus backscattered radiation), SSA (a measure of the absorption by the aerosol), and aerosol size distributions (Dubovik et al. 2000).

b. Multifilter rotating shadowband radiometer

Several variants of the MFRSR are used in the ARM Program. The MFRSR was developed with ARM funding in the early 1990s (Harrison et al. 1994) and was licensed to Yankee Environmental Systems, Inc., in the mid-1990s. While the Cimel is a traditional pointing sunphotometer with a 1.2° field of view and a filter wheel that cycles to sequentially sample all nine channels, the MFRSR makes simultaneous measurements in seven temperature-controlled channels. The GHI is measured with the rotating band out of the field of view. The band rotates about an axis parallel to Earth's rotation allowing the required steps in hour angle to be calculated to block the diffuser from direct solar radiation in order to measure the DHI (http://yesinc.com/products/radvis.html). Finally, the DNI is calculated from these two measurements [see Harrison et al. (1994) for complete details]. Six of these channels contain 10-nm filters; five are used for AOD measurements and one for water vapor. The seventh channel is an unfiltered silicon detector that is used to estimate broadband solar after corrections for spectral response are applied. This unfiltered channel's measurements can be used as backup to the broadband thermopile measurements of shortwave irradiance.

The MFRSR samples wavelengths at 415, 500, 615, 673, and 870 nm for AOD determinations. Instruments are calibrated for AOD retrievals after first screening all of the data for acceptable Langley plots as outlined in Harrison and Michalsky (1994). Robust estimates of the calibration constants using all of the acceptable Langley plots are obtained following the procedures described in Michalsky et al. (2001), which provide uncertainties in the derived AOD, due to uncertainties in calibration, of 0.01 to 0.02. These methods use field measurements to continuously update the calibration; therefore, the instruments are not removed from the field for calibration unless there is an instrument failure. Several studies (e.g., Michalsky et al. 2010) have compared the Cimel sunphotometer estimates of AOD with the MFRSR AODs and found results clearly within the uncertainties cited above. In that paper, a 15-yr AOD climatology (through the early part of 2008) was produced for the SGP aerosols based on the continuous monitoring possible using the field calibration procedure just outlined; the importance of this result is discussed in McComiskey and Ferrare (2016, chapter 21). Although the 940-nm channel measurements are made, the data have not been used to routinely retrieve water vapor in the ARM Program, although comparisons with other methods to retrieve precipitable water vapor have been performed (e.g., Alexandrov et al. 2008, and references therein; Turner et al. 2016, chapter 13). The MFRSR sampling is every 20 s although some early data were sampled every 15 s. While Cimel almucanter and solar-zenith plane scans are used to retrieve AP and SSA, as explained above, the MFRSR diffuse and direct irradiances are used in a different procedure to retrieve the same parameters. Kassianov et al. (2007) demonstrated these retrievals for AP and SSA and compared their retrievals with in situ techniques and AERONET retrievals with good agreement. The most extensive effort to use MFRSRs for the characterization of aerosols was by Alexandrov and his colleagues at the Goddard Institute for Space Studies in New York City (Alexandrov et al. 2008, and many references therein). Their focus was on retrieving size distributions including the separation of fine and coarse modes. They found good agreement when comparing derivations using two different MFRSRs and when comparing MFRSR retrievals to the Cimel sun–sky-based retrievals.

A key input for the retrieval of the SSA and AP is the spectral albedo of the land surface. Later in this chapter we note that surface albedo is key to deriving cloud

optical depths. As discussed earlier in this chapter, surface spectral albedo was a key factor in achieving radiative closure between clear-sky broadband models and measurements (Michalsky et al. 2006). The albedo measurements used for that study were made with the MFRSR for downwelling irradiance; the upwelling measurements were made with the detector head of the MFRSR, the MFR. The filters for the MFR and MFRSR are at the same wavelengths. At the SGP central facility one MFR is placed near the top of a 10-m tower not far from the MFRSRs. This site is pastureland and is considered representative of fallow land around the ARM site. Another MFR is sited at the 25-m level of the 60-m meteorological tower that is within a cultivated field some 350 m WNW of the 10-m tower. This field was planted mostly with winter wheat in the early years of ARM, but after the fall of 2004 corn, soybeans, and wheat have been rotated (McFarlane et al. 2011). The field is tilled before planting and after harvest revealing bare soil until weeds or planted crops emerge. McFarlane et al. (2011) developed a value added product (VAP), useful in radiative transfer calculations, to derive a continuous surface spectral albedo dataset using the MFRs and MFRSRs plus a calculation of Normalized Difference Vegetative Index (NDVI) from these albedos to provide an understanding of the surface type.

c. *Normal incidence multifilter radiometer*

Two straightforward modifications of the MFRSR were made for specific purposes in ARM. The normal incidence multifilter radiometer (NIMFR) has the same filter-detector package as the MFRSR, but is equipped with a baffled tube to restrict the field of view to 5.7° to match the Eppley model NIP pyrheliometer. Samples in all channels are obtained simultaneously every 20 s. It is calibrated in the same way as the MFRSR using multiple Langley regressions and deriving a robust estimate of the extraterrestrial response for each aerosol channel from these. The AODs derived from the NIMFR should have less uncertainty than those obtained with the MFRSR because there are no cosine response corrections to apply, which add uncertainty. Michalsky et al. (2010) show agreement within 0.014 with the MFRSR, which is slightly better than the agreement of the MFRSR with AERONET, since the sampling and wavelengths are better matched in the former case.

8. Spectral solar measurements for cloud retrievals

a. *Multifilter rotating shadowband radiometer*

The MFRSR can be used to measure cloud optical depths for totally overcast skies filled with water clouds (no ice). The instrument is calibrated when the sky is cloud free using Langley plots as described earlier, which calibrates the direct beam for top-of-the-atmosphere response. Moreover, the calibration applies to the diffuse and global irradiance as well, since the same sensor is used in all three measurements. Measurements of irradiance under clouds then can be used to calculate the transmission by taking the ratio of this measurement to the top-of-the-atmosphere global irradiance (i.e., the direct irradiance multiplied by the cosine of the solar zenith angle). A radiative transfer model that has estimated or measured surface albedo and assumed or obtained independently cloud droplet radius can be run iteratively changing the optical depth until the transmission matches the measurement. Min and Harrison (1996) have shown that there is only a small added uncertainty in the cloud optical depth if a fixed reasonable estimate of cloud droplet radius is assumed. Their procedure uses measurements at the shortest MFRSR wavelength, 415 nm, because the surface albedo is low there, and small differences from the true value have little effect on the estimated cloud optical depth. If the liquid water path is measured by a collocated microwave radiometer (see, e.g., Shupe et al. 2016, chapter 19), then this algorithm can retrieve the cloud droplet radius and produce an improved estimate of the cloud optical depth. In later studies, Min et al. (2008) demonstrated the retrieval of cloud fraction from spectral measurements made with the MFRSR. Wang and Min (2008) further developed methods to retrieve thin and mixed-phase cloud optical depths using the MFRSR.

b. *Two-channel narrow field-of-view and Cimel radiometers in cloud mode*

The narrow field-of-view (NFOV) radiometer was developed to measure zenith radiances at 1-s temporal resolution with two channels, one in the red (673 nm) and one in the near-infrared (870 nm), for the purpose of retrieving cloud properties. Cloud optical properties at these two wavelengths are nearly identical, but green vegetative surfaces reflect these two wavelengths very differently. This instrument uses some MFRSR technology, but is different in that it does not use a diffuser over the two separate receivers since that would cut the signal to unusably low levels. This instrument also uses higher gain for the low radiance signals. The current field of view is 1.2°, down from the original 5.7°, with the smaller field of view matching the Cimel, allowing comparisons of the two instruments' cloud retrievals. This smaller field of view allows successful sampling of geometrically smaller clouds; for the technique to work the cloud must fill the field of view. Chiu et al. (2006) demonstrated that 1-s data captures the frequency at

which clouds evolve naturally. They estimate that cloud optical depths using this technique are measured with an uncertainty of about 15%. Chiu et al. (2012) recently used the ARM Cimel in its zenith radiance mode measuring with visible and near-infrared (1640 nm) wavelengths to retrieve cloud optical depth, effective cloud droplet radius, and liquid water path.

9. The future of broadband and narrowband radiometry in ARM

Remarkable improvements have been made in the accuracy of radiation measurements over the past 20 years based on research in the ARM Program and BSRN. The DNI was measured with good accuracy before, but the accuracy of commercial pyrheliometers is now better understood (Michalsky et al. 2001). These DNI measurements can now be made with accuracies of 0.7% using an all-weather instrument. The measurement of DHI is much better now since a procedure to produce a DHI standard has been developed (Michalsky et al. 2007); DHI accuracies of around 2% are possible. Infrared measurements have shown the most improvement. IPASRC I/II studies conducted at SGP and NSA were pivotal in establishing the WISG. These measurements can be made at the 2%–3% level, where they were at about the 10% uncertainty level at the outset of the ARM Program.

a. Multifilter rotating shadowband radiometer

MFRSRs were refurbished with new filters and better temperature control in the late 2000s. The new filter sets have better throughput resulting in better signal-to-noise ratios. Close attention was paid to reducing the out-of-band light getting through the filters, which was adding nonnegligible uncertainty to AOD retrievals. The temperature is controlled very closely near the set point except on a few hot summer days when the internal temperature exceeds the set point; the improved temperature control improves the calibration stability of the instrument for long time periods between successful Langley calibrations. A Campbell datalogger controls the MFRSR, allowing them to be operated in more flexible modes. ARM is considering a slight change to the filter set where the 615-nm channel would be swapped for a 1625-nm channel to enable several new scientific studies, and the feasibility of this change has been demonstrated. This change would permit a better estimate of the shortwave surface albedo in the near-infrared; it would allow a two-channel retrieval of cloud optical depth and cloud particle radius simultaneously, and it would allow a better retrieval of large aerosol sizes.

b. Broadband

In the comparison of pyrheliometers reported in section 6b (Michalsky et al. 2011) it was found that the current ARM pyrheliometers measured direct irradiance with an estimated accuracy of 1.3% within 95% confidence limits. It would seem prudent to upgrade the ARM pyrheliometers to one of the instruments in that comparison that measured with an accuracy near 0.7%. This would result in a substantial uncertainty improvement of the measurements since direct beam is the largest contributor to downwelling shortwave irradiance.

Infrared measurements should improve significantly with the impending improvement in the calibration procedure. Outdoor calibrations to the WISG should reduce the absolute uncertainty of these measurements to around $\pm 5\,\mathrm{W\,m^{-2}}$. Given the long-term stability of the Eppley model PIR, the calibrations should be valid from the earliest measurements in ARM. This will allow for an interesting analysis of surface net infrared changes over the past 20 years in the case of the SGP and NSA central facilities.

Acknowledgments. Anthony Bucholtz, Dave Turner, and an anonymous referee offered insightful comments that led to considerable improvement of the final version of this chapter.

REFERENCES

Ackerman, T. P., D. M. Flynn, and R. T. Marchand, 2003: Quantifying the magnitude of anomalous solar absorption. *J. Geophys. Res.*, **108**, 4273, doi:10.1029/2002JD002674.

Alexandrov, M. D., A. A. Lacis, B. E. Carlson, and B. Cairns, 2008: Characterizations of atmospheric aerosols using MFRSR measurements. *J. Geophys. Res.*, **113**, D08204, doi:10.1029/2007JD009388.

Asano, S., A. Uchiyama, Y. Mano, M. Murakami, and Y. Takayama, 2000: No evidence for solar absorption anomaly by marine water clouds through collocated aircraft radiation measurements. *J. Geophys. Res.*, **105**, 14 761–14 775, doi:10.1029/2000JD900062.

Barnard, J. C., C. N. Long, E. I. Kassianov, S. A. McFarlane, J. M. Comstock, M. Freer, and G. M. McFarquhar, 2008: Development and evaluation of a simple algorithm to find cloud optical depth with emphasis on thin ice clouds. *Open Atmos. Sci. J.*, **2**, 46–55, doi:10.2174/1874282300802010046.

Berg, L. K., E. I. Kassianov, C. N. Long, and D. L. Mills Jr., 2011: Surface summertime radiative forcing by shallow cumuli at the Atmospheric Radiation Measurement Southern Great Plains site. *J. Geophys. Res.*, **116**, D01202, doi:10.1029/2010JD014593.

Bush, B. C., F. P. J. Valero, A. S. Simpson, and L. Bignone, 2000: Characterization of thermal effects in pyranometers: A data correction algorithm for improved measurement of surface insolation. *J. Atmos. Oceanic Technol.*, **17**, 165–175, doi:10.1175/1520-0426(2000)017<0165:COTEIP>2.0.CO;2.

Cess, R. D., and Coauthors, 1995: Absorption of solar radiation by clouds: Observations versus models. *Science*, **267**, 496–499, doi:10.1126/science.267.5197.496.

Chiu, J. C., A. Marshak, Y. Knyazikhin, W. J. Wiscombe, H. W. Barker, J. C. Barnard, and Y. Luo, 2006: Remote sensing of cloud properties using ground-based measurements of zenith radiance. *J. Geophys. Res.*, **111**, D16201, doi:10.1029/2005JD006843.

——, and Coauthors, 2012: Cloud droplet size and liquid water path retrievals from zenith radiance measurements: Examples from the Atmospheric Radiation Measurement Program and the Aerosol Robotic Network. *Atmos. Chem. Phys.*, **12**, 10 313–10 329, doi:10.5194/acp-12-10313-2012.

Clough, S. A., and Coauthors, 2000: A longwave broadband QME based on ARM pyrometer and AERI measurements. *Extended Abstracts, 10th ARM Science Team Meeting*, San Antonio, TX, ARM Program. [Available online at http://www.arm.gov/publications/proceedings/conf10/extended_abs/clough_sa.pdf.]

Coulson, K. L., and Y. Howell, 1980: Solar radiation instruments. *Sunworld*, **4**, 87–94.

Dong, X., B. Xi, K. Crosby, C. N. Long, R. S. Stone, and M. D. Shupe, 2010: A 10 year climatology of Arctic cloud fraction and radiative forcing at Barrow, Alaska. *J. Geophys. Res.*, **115**, D17212, doi:10.1029/2009JD013489.

Dubovik, O., A. Smirnov, B. N. Holben, M. D. King, Y. J. Kaufman, T. F. Eck, and I. Slutsker, 2000: Accuracy assessments of aerosol optical properties retrieved from Aerosol Robotic Network (AERONET) sun and sky radiance measurements. *J. Geophys. Res.*, **105**, 9791–9806, doi:10.1029/2000JD900040.

Dürr, B., and R. Philipona, 2004: Automatic cloud amount detection by surface longwave downward radiation measurements. *J. Geophys. Res.*, **109**, D05201, doi:10.1029/2003JD004182.

Dutton, E. G., J. J. Michalsky, T. Stoffel, B. W. Forgan, J. Hickey, D. W. Nelson, T. L. Alberta, and I. Reda, 2001: Measurement of broadband diffuse solar irradiance using current commercial instrumentation with a correction for thermal offset errors. *J. Atmos. Oceanic Technol.*, **18**, 297–314, doi:10.1175/1520-0426(2001)018<0297:MOBDSI>2.0.CO;2.

Ellingson, R. G., and W. J. Wiscombe, 1996: The Spectral Radiance Experiment (SPECTRE): Project description and sample results. *Bull. Amer. Meteor. Soc.*, **77**, 1967–1985, doi:10.1175/1520-0477(1996)077<1967:TSREPD>2.0.CO;2.

——, J. Ellis, and S. Fels, 1991: The intercomparison of radiation codes used in climate models: Longwave results. *J. Geophys. Res.*, **96**, 8929–8953, doi:10.1029/90JD01450.

Fouquart, Y., B. Bonnel, and V. Ramaswamy, 1991: Intercomparing shortwave radiation codes for climate studies. *J. Geophys. Res.*, **96**, 8955–8968, doi:10.1029/90JD00290.

Francis, P. N., J. P. Taylor, P. Hignett, and A. Slingo, 1997: On the question of enhanced absorption of solar radiation by clouds. *Quart. J. Roy. Meteor. Soc.*, **123**, 419–434, doi:10.1002/qj.49712353809.

Fröhlich, C., R. Philipona, J. Romero, and C. Wehrli, 1995: Radiometry at the Physikalisch-Meteorologisches Observatorium Davos and World Radiation Centre. *Opt. Eng.*, **34**, 2757–2766, doi:10.1117/12.205682.

Gregory, L., 2011: Cimel Sunphotometer (CSPHOT) Handbook. ARM Tech. Rep. DOE/SC-ARM TR-056, 17 pp. [Available online at https://www.arm.gov/instruments/csphot.]

Gulbrandsen, A., 1978: On the use of pyranometers in the study of spectral solar radiation and atmospheric aerosols. *J. Appl. Meteor.*, **17**, 899–904, doi:10.1175/1520-0450(1978)017<0899:OTUOPI>2.0.CO;2.

Halthore, R. N., S. Nemesure, S. E. Schwartz, D. G. Imre, A. Berk, E. G. Dutton, and M. H. Bergin, 1998: Models overestimate diffuse clear-sky surface irradiance: A case for excess atmospheric absorption. *Geophys. Res. Lett.*, **25**, 3591–3594, doi:10.1029/98GL52809.

——, M. A. Miller, J. A. Ogren, P. J. Sheridan, D. W. Slater, and T. Stoffel, 2004: Further developments in closure experiments for the surface diffuse irradiance under cloud-free skies at a continental site. *Geophys. Res. Lett.*, **31**, L07111, doi:10.1029/2003GL019102.

Harrison, L., and J. Michalsky, 1994: Objective algorithms for the retrieval of optical depths from ground-based measurements. *Appl. Opt.*, **33**, 5126–5132, doi:10.1364/AO.33.005126.

——, ——, and J. Berndt, 1994: Automated multifilter rotating shadow-band radiometer: An instrument for optical depth and radiation measurements. *Appl. Opt.*, **33**, 5118–5125, doi:10.1364/AO.33.005118.

Holben, B. N., and Coauthors, 1998: AERONET—A federated instrument network and data archive for aerosol characterization. *Remote Sens. Environ.*, **66**, 1–16, doi:10.1016/S0034-4257(98)00031-5.

IPCC, 2007: *Climate Change 2007: The Physical Science Basis*. Cambridge University Press, 996 pp.

Kassianov, E., C. J. Flynn, T. P. Ackerman, and J. C. Barnard, 2007: Aerosol single-scattering albedo and asymmetry parameter form MFRSR observations during the ARM aerosol IOP 2003. *Atmos. Chem. Phys.*, **7**, 3341–3351, doi:10.5194/acp-7-3341-2007.

Kato, S., T. P. Ackerman, E. E. Clothiaux, J. H. Mather, G. G. Mace, M. L. Wesely, F. Murcray, and J. Michalsky, 1997: Uncertainties in modeled and measured clear-sky surface shortwave irradiances. *J. Geophys. Res.*, **102**, 25 881–25 898, doi:10.1029/97JD01841.

Kerr, R. A., 2003: Making clouds darker sharpens cloudy climate models. *Science*, **300**, 1859–1860, doi:10.1126/science.300.5627.1859a.

Knuteson, R. O., and Coauthors, 2004: The Atmospheric Emitted Radiance Interferometer (AERI) Part I: Instrument design. *J. Atmos. Oceanic Technol.*, **21**, 1763–1776, doi:10.1175/JTECH-1662.1.

Long, C. N., 2005: On the estimation of clear-sky upwelling shortwave and longwave. *Extended Abstracts, 15th ARM Science Team Meeting*, Daytona Beach, FL, ARM Program. [Available online at http://www.arm.gov/publications/proceedings/conf15/extended_abs/long_cn.pdf.]

——, and T. P. Ackerman, 2000: Identification of clear skies from broadband pyranometer measurements and calculation of downwelling shortwave cloud effects. *J. Geophys. Res.*, **105**, 15 609–15 626, doi:10.1029/2000JD900077.

——, and D. D. Turner, 2008: A method for continuous estimation of clear-sky downwelling longwave radiative flux developed using ARM surface measurements. *J. Geophys. Res.*, **113**, D18206, doi:10.1029/2008JD009936.

——, T. P. Ackerman, K. L. Gaustad, and J. N. S. Cole, 2006: Estimation of fractional sky cover from broadband shortwave radiometer measurements. *J. Geophys. Res.*, **111**, D11204, doi:10.1029/2005JD006475.

——, E. G. Dutton, J. A. Augustine, W. Wiscombe, M. Wild, S. A. McFarlane, and C. J. Flynn, 2009: Significant decadal brightening of downwelling shortwave in the continental United States. *J. Geophys. Res.*, **114**, D00D06, doi:10.1029/2008JD011263.

Mace, G. G., and Coauthors, 2006: Cloud radiative forcing at the Atmospheric Radiation Measurement Program Climate Research Facility: 1. Technique, validation, and comparison to

satellite-derived diagnostic quantities. *J. Geophys. Res.*, **111**, D11S90, doi:10.1029/2005JD005921.

Marty, C., and Coauthors, 2003: Downward longwave irradiance uncertainty under Arctic atmospheres: Measurements and modeling. *J. Geophys. Res.*, **108**, 4358, doi:10.1029/2002JD002937.

May, P. T., C. N. Long, and A. Protat, 2012: The diurnal cycle of the boundary layer, convection, clouds, and surface radiation in a coastal monsoon environment (Darwin, Australia). *J. Climate*, **25**, 5309–5326, doi:10.1175/JCLI-D-11-00538.1.

McComiskey, A., and R. A. Ferrare, 2016: Aerosol physical and optical properties in the ARM Program. *The Atmospheric Radiation Measurement (ARM) Program: The First 20 Years, Meteor. Monogr.*, No. 57, Amer. Meteor. Soc., doi:10.1175/AMSMONOGRAPHS-D-15-0028.1.

McFarlane, S. A., K. L. Gaustad, E. J. Mlawer, C. N. Long, and J. Delamere, 2011: Development of a high spectral resolution surface albedo product for the ARM Southern Great Plains central facility. *Atmos. Meas. Tech.*, **4**, 1713–1733, doi:10.5194/amt-4-1713-2011.

——, C. N. Long, and J. Flaherty, 2013: A climatology of surface cloud radiative effects at the ARM Tropical Western Pacific sites. *J. Appl. Meteor. Climatol.*, **52**, 996–1013, doi:10.1175/JAMC-D-12-0189.1.

——, J. H. Mather, and E. J. Mlawer, 2016: ARM's progress on improving atmospheric broadband radiative fluxes and heating rates. *The Atmospheric Radiation Measurement (ARM) Program: The First 20 Years, Meteor. Monogr.*, No. 57, Amer. Meteor. Soc., doi:10.1175/AMSMONOGRAPHS-D-15-0046.1.

Michalsky, J. J., J. Schlemmer, W. Berkheiser III, J. Berndt, L. Harrison, N. Laulainen, N. Larson, and J. Barnard, 2001: Multiyear measurements of aerosol optical depth in the Atmospheric Radiation Measurement and Quantitative Links programs. *J. Geophys. Res.*, **106**, 12 099–12 107, doi:10.1029/2001JD900096.

——, and Coauthors, 2002: Broadband shortwave calibration results from the Atmospheric Radiation Measurement Enhanced Shortwave Experiment II. *J. Geophys. Res.*, **107** (D16), doi:10.1029/2001JD001231.

——, and Coauthors, 2003: Results from the first ARM diffuse horizontal shortwave irradiance comparison. *J. Geophys. Res.*, **108**, 4108, doi:10.1029/2002JD002825.

——, and Coauthors, 2005: Toward the development of a diffuse horizontal shortwave irradiance working standard. *J. Geophys. Res.*, **110**, D06107, doi:10.1029/2004JD005265.

——, and Coauthors, 2006: Shortwave radiative closure studies for clear skies during the Atmospheric Radiation Measurement 2003 Aerosol Intensive Observation Period. *J. Geophys. Res.*, **111**, D14S90, doi:10.1029/2005JD006341.

——, C. Gueymard, P. Kiedron, L. J. B. McArthur, R. Philipona, and T. Stoffel, 2007: A proposed working standard for the measurement of diffuse horizontal shortwave irradiance. *J. Geophys. Res.*, **112**, D16112, doi:10.1029/2007JD008651.

——, F. Denn, C. Flynn, G. Hodges, P. Kiedron, A. Koontz, J. Schlemmer, and S. E. Schwartz, 2010: Climatology of aerosol optical depth in north-central Oklahoma: 1992–2008. *J. Geophys. Res.*, **115**, D07203, doi:10.1029/2009JD012197.

——, and Coauthors, 2011: An extensive comparison of commercial pyrheliometers under a wide range of routine observing conditions. *J. Atmos. Oceanic Technol.*, **28**, 752–766, doi:10.1175/2010JTECHA1518.1.

Min, Q., and L. C. Harrison, 1996: Cloud properties derived from surface MFRSR measurements and comparison with GOES results at the ARM SGP site. *Geophys. Res. Lett.*, **23**, 1641–1644, doi:10.1029/96GL01488.

——, T. Wang, C. N. Long, and M. Duan, 2008: Estimating fractional sky cover from spectral measurements. *J. Geophys. Res.*, **113**, D20208, doi:10.1029/2008JD010278.

Mlawer, E. J., and D. D. Turner, 2016: Spectral radiation measurements and analysis in the ARM Program. *The Atmospheric Radiation Measurement (ARM) Program: The First 20 Years, Meteor. Monogr.*, No. 57, Amer. Meteor. Soc., doi:10.1175/AMSMONOGRAPHS-D-15-0027.1.

Myers, D. R., T. L. Stoffel, I. Reda, S. M. Wilcox, and A. Andreas, 2002: Recent progress in reducing the uncertainty in and improving pyranometer calibrations. *J. Solar Energy. Eng.*, **124**, 44–49, doi:10.1115/1.1434262.

Ohmura, A., and Coauthors, 1998: Baseline Surface Radiation Network (BSRN/WCRP): New precision radiometry for climate research. *Bull. Amer. Meteor. Soc.*, **79**, 2115–2136, doi:10.1175/1520-0477(1998)079<2115:BSRNBW>2.0.CO;2.

Philipona, R., and Coauthors, 2001: Atmospheric longwave irradiance uncertainty: Pyrgeometers compared to an absolute sky-scanning radiometer, atmospheric emitted radiance interferometer, and radiative transfer model calculations. *J. Geophys. Res.*, **106**, 28 129–28 141, doi:10.1029/2000JD000196.

Pilewskie, P., and F. P. J. Valero, 1995: Direct observations of excess absorption by clouds. *Science*, **267**, 1626–1629, doi:10.1126/science.267.5204.1626.

Qian, Y., C. N. Long, H. Wang, J. Comstock, S. A. McFarlane, and S. Xie, 2012: Evaluation of cloud fraction and its radiative effect simulated by IPCC AR4 global models against ARM surface observations. *Atmos. Chem. Phys.*, **12**, 1785–1810, doi:10.5194/acp-12-1785-2012.

Ramanathan, V., B. Subasilar, B, G. J. Zhang, W. Conant, R. D. Cess, J. T. Kiehl, H. Grassl, and L. Shi, 1995: Warm pool heat budget and shortwave cloud forcing: A missing physics? *Science*, **267**, 499–503, doi:10.1126/science.267.5197.499.

Reda, I., and T. Stoffel, 2001: Pyrgeometer calibrations at NREL. *Proc. 11th ARM Science Team Meeting*, Atlanta, GA, ARM Program. [Available online at http://www.arm.gov/publications/proceedings/conf11/poster_abs/P00005.]

Ricchiazzi, P., S. Yang, C. Gautier, and D. Sowle, 1998: SBDART: A research and teaching software tool for plane-parallel radiative transfer in the Earth's atmosphere. *Bull. Amer. Meteor. Soc.*, **79**, 2101–2114, doi:10.1175/1520-0477(1998)079<2101:SARATS>2.0.CO;2.

Shupe, M. D., J. M. Comstock, D. D. Turner, and G. G. Mace, 2016: Cloud property retrievals in the ARM Program. *The Atmospheric Radiation Measurement (ARM) Program: The First 20 Years, Meteor. Monogr.*, No. 57, Amer. Meteor. Soc., doi:10.1175/AMSMONOGRAPHS-D-15-0030.1.

Stoffel, T., I. Reda, J. Hickey, E. Dutton, and J. Michalsky, 2006: Pyrgeometer calibrations for the Atmospheric Radiation Measurement Program: Updated approach. *Extended Abstracts, 16th ARM Science Team Meeting*, Albuquerque, NM, ARM Program. [Available online at http://www.arm.gov/publications/proceedings/conf16/extended_abs/stoffel_t.pdf.]

Turner, D. D., and Coauthors, 2004: The QME AERI LBLRTM: A closure experiment for downwelling high spectral resolution infrared radiance. *J. Atmos. Sci.*, **61**, 2657–2675, doi:10.1175/JAS3300.1.

——, E. J. Mlawer, and H. E. Revercomb, 2016: Water vapor observations in the ARM Program. *The Atmospheric Radiation Measurement (ARM) Program: The First 20 Years,*

Meteor. Monogr., No. 57, Amer. Meteor. Soc., doi:10.1175/AMSMONOGRAPHS-D-15-0025.1.

Valero, F. P. J., A. Bucholtz, B. C. Bush, S. K. Pope, W. D. Collins, P. Flatau, A. Strawa, and W. J. Y. Gore, 1997a: Atmospheric Radiation Measurements Enhanced Shortwave Experiment (ARESE): Experimental and data details. *J. Geophys. Res.*, **102**, 29 929–29 937, doi:10.1029/97JD02434.

——, R. D. Cess, M. Zhang, S. K. Pope, A. Bucholtz, B. Bush, and J. Vitko, 1997b: Absorption of solar radiation by the cloudy atmosphere: Interpretations of collocated aircraft measurements. *J. Geophys. Res.*, **102**, 29 917–29 927, doi:10.1029/97JD01782.

——, and Coauthors, 2003: Absorption of solar radiation by the clear and cloudy atmosphere during the Atmospheric Radiation Measurement Enhanced Shortwave Experiments (ARESE) I and II: Observations and models. *J. Geophys. Res.*, **108**, 4016, doi:10.1029/2001JD001384.

Vignola, F., J. Michalsky, and T. Stoffel, 2012: *Solar and Infrared Radiation Measurements.* CRC Press, 410 pp.

Wang, T., and Q. Min, 2008: Retrieving optical depths of optically thin and mixed-phase clouds from MFRSR measurements. *J. Geophys. Res.*, **113**, D19203, doi:10.1029/2008JD009958.

Wang, Y., C. N. Long, J. H. Mather, and X. D. Liu, 2011: Convective signals from surface measurements at ARM Tropical Western Pacific site: Manus. *Climate Dyn.*, **36**, 431–449, doi:10.1007/s00382-009-0736-z.

Wild, M., C. N. Long, and A. Ohmura, 2006: Evaluation of clear-sky solar fluxes in GCMs participating in AMIP and IPCC-AR4 from a surface perspective. *J. Geophys. Res.*, **111**, D01104, doi:10.1029/2005JD006118.

Younkin, K., and C. N. Long, 2004: Improved correction of IR loss in diffuse shortwave measurements: An ARM value added product. ARM Tech. Rep. ARM TR-009, 47 pp.

Zender, C. S., B. Bush, S. K. Pope, A. Bucholtz, W. D. Collins, J. T. Kiehl, F. P. J. Valero, and J. Vitko, 1997: Atmospheric absorption during the Atmospheric Radiation Measurement (ARM) Enhanced Shortwave Experiment (ARESE). *J. Geophys. Res.*, **102**, 29 901–29 915, doi:10.1029/97JD01781.

Zhang, Y., C. N. Long, W. B. Rossow, and E. G. Dutton, 2010: Exploiting diurnal variations to evaluate the ISCCP-FD flux calculations and radiative-flux-analysis-processed surface observations from BSRN, ARM and SURFRAD. *J. Geophys. Res.*, **115**, D15105, doi:10.1029/2009JD012743.